Preprint Manuscript:
Zhang, Z., Huang, Y. & Bridgelall, R. Vehicle axle detection from under-sampled signal through compressed-sensing-based signal recovery. J Civil Struct Health Monit (2022).
https://doi.org/10.1007/s13349-022-00601-4

Vehicle Axle Detection from Under-Sampled Signal through Compressed-Sensing Based Signal Recovery

Zhiming Zhang[a], Ying Huang[b], Raj Bridgelall[c]

[a] *School for Engineering of Matter, Transport and Energy, Arizona State University, USA*
[b] *Civil and Environmental Engineering Department, North Dakota State University, USA*
[c] *College of Business, North Dakota State University, USA*
[d] *Upper Great Plains Transportation Institute (UGPTI), North Dakota State University, USA*

Abstract

In traffic data collection, sampling design should satisfy the requirements of identifying prominent pulses corresponding to vehicle axle passage. Insufficient measurement leads to signal distortion and attenuation, reducing the quality of signal pulses. This study exploits the value of under-sampled data by applying compressed sensing (CS) methods to recover signal components that are critical for vehicle axle detection. Two CS methods are investigated in this study to recover the strain signal pulses from inside-pavement instrumented sensors at high-speed traversals. The CS methods successfully recovered the signal pulses from all axles of the truck used for testing. A comparison of the measured axle distances with the reference measurements validated the effectiveness of signal recovery methods. Therefore, the CS methods have the potential of reducing the cost, energy consumption, and data storage space, and improving the data transmission efficiency in practical implementations by enabling sampling devices designed for static measurements to achieve dynamic measurements.

Keywords: vehicle axle detection, compressed sensing, under-sampling, signal recovery

1. Introduction

Vehicle axle detection plays a significant role in traffic data collection including vehicle counting, vehicle classification, and vehicle speed measurement [1–3]. Technologies performing vehicle axle detection fall into the categories of intrusive sensing (e.g., inductive loops, piezoelectric cables, and fiber optic sensors) and non-intrusive sensing (e.g., infrared, microwave radar, and vehicle imaging) [2]. Many of the sensors are constituents of traffic control and management system that consists of multiple application modules [4].

Available technologies measure signals using optical, acoustical, or photographic methods to identify the passage of vehicle axles. A sufficient sampling frequency of the measurement

Email addresses: `corresponding author: zzhan506@asu.edu` (Zhiming Zhang), `ying.huang@ndsu.edu` (Ying Huang), `raj.bridgelall@ndsu.edu` (Raj Bridgelall)

device is required to achieve satisfactory signal quality without much signal distortion and guarantee measurement accuracy [5, 6]. By analyzing in-pavement strain signals excited with vehicle passes, the work presented in [5] showed that insufficient sampling (i.e., under-sampling) will lead to severe signal distortion. Signal distortion merges signal pulses for adjacent axles and thus prevents accurate axle detection. Nevertheless, a redundantly high sampling frequency in traffic data collection leads to potential energy and storage waste. Axle detection using under-sampled data is desirable to relieve the cost for data transmission and the required space for data storage.

Compressed sensing (CS) has the potential of identifying the merged signal pulses from severely distorted signals. CS recovers under-sampled signals via optimization. CS has been wildly applied in biology, medicine, astronomy, etc. since its initiation in [7] and [8]. However, its application in traffic data analysis is very limited. Zhang et al. [9] used CS methods to recover in-pavement strain signals for weigh-in-motion (WIM) measurements. Sousa and Wang [10] used CS methods to reconstruct strain measurements on bridges. Nevertheless, none of them applies the CS technique to recover signals corresponding to respective vehicle passes, which is important for the comprehensive traffic analysis and infrastructure maintenance.

In the present study, CS methods will be applied to recover the insufficiently measured traffic data for vehicle axle detection via analyzing the properties of traffic-induced in-pavement strain signals and specifically designing the method details for this signal recovery problem, including the sensing matrix, sparsity level, upsampling ratio, etc. The new contributions of the proposed method are:

1. Vehicle axle detection from under-sampled signal is investigated via CS based signal recovery.
2. The CS problem is mathematically formulated (including the sensing matrix, expansion matrix, wavelet basis, etc.) for signal recovery from under-sampled signal, which can be extended to other practical applications.
3. Signal pulses important for vehicle axle identification can be successfully extracted via CS, which is validated via experimental studies.
4. Two CS methods (i.e., CoSaMP and LASSO methods) are compared to find the most efficient approach for vehicle axle detection.

The structure of the remaining part of the present paper is: in Section 2, the basics of CS methods for signal recovery are introduced. Section 3 introduces the measured signals used for the evaluation and analyzes the signals' properties. Section 4 formulates the CS problem for axle detection by deriving the sensing matrix and analyzes the measured signal with sufficient sampling frequency for axle detection. Section 5 applies the two CS methods and analyzes their efficiency in recovering accurate signals for axle detection. In Section 6, the conclusions elaborate that the CS methods can be used to recover signals from under-sampled measurements with satisfactory accuracy for direct axle detection.

2. Basics of CS Methods

In the CS theory, the original signals can be reconstructed using reduced/downsampled measurements as long as their sparseness and/or compressibility satisfy certain conditions [7, 11, 12]. With signals compressed at a sampling rate that is much lower than required in the traditional practice according to the sampling theorem, CS can potentially improve the efficiency of data transmission and decrease the space for data storage.

$x = (x_i)_{i=1}^n \in \mathbb{R}^n$ is the signal to be recovered via CS. Usually, x itself is not a sparse signal for CS. It is assumed that an orthonormal basis Ψ exits, so that $x = \Psi s$ with s being a sparse vector. Φ is the sensing matrix or measurement matrix with a dimension of $m \times n$. In CS, it is assumed that $m < n$. Then the CS problem becomes recovering s from the measured signal $y = \Phi\Psi s$ or $y = \Theta s$, in which $\Theta = \Phi\Psi$ [13, 14]. Three types of algorithms are available to solve the CS problem, namely, (1) Greedy pursuits, (2) Convex relaxation, and (3) Combinatorial algorithms. Every category of algorithms has its advantages as well as shortcomings [15]. Combinatorial algorithms are computationally fast but demanding regarding the amount of data. In comparison, convex relaxation algorithms has much less requirement on data quantity while they are less computationally efficient. Greedy pursuits are intermediate in these two aspects compared with the combinatorial and convex relaxation algorithms. For comparison, this study applies a method with greedy pursuits, the Compressive Sampling Matching Pursuit (CoSaMP) method, and a convex relaxation method, the LASSO method, to reconstruct the vehicle-induced signals using the insufficiently measured strain data from in-pavement embedded sensors.

(a) (b)

Figure 1: MnROAD Facility at MnDOT. (a) the road sections managed by the MnROAD Facility; (b) the concrete road section.

CoSaMP is essentially a greedy pursuit. Compraed with other greed pursuits, its computational speed and rigorous error bounds are guaranteed by borrowing ideas from combinatorial algorithms [17]. In CoSaMP, an approach inspired by the restricted isometry property is used to conduct the most challenging step of signal reconstruction, i.e., determining the locations of the target signal's largest components. In detail, the vector $y^* = \Phi^*\Phi x$ is taken as a proxy for the signal, which is approximated by applying the matrix Φ^* to the collected samples. This idea is implemented iteratively in the CoSaMP algorithm to approximate the target signal, yielding an approximation residual in each iteration. In each iteration, samples are updated using the present residual, following which the signal proxy is updated and the largest components identified. The iteration is repeated until the signal energy is recovered. Compared with other greedy algorithms, CoSaMP has improved computational efficiency by identifying more than one largest component in each iteration.

As a convex optimization method, the LASSO approach has few constraint on the objective functions. For example, the cardinality does not need to be known in advance in LASSO. In LASSO, with the assumptipn that x is sparse, the L1-norm regularization is incorporated into the objective function to supress non-contributive elements in x. The CS problem is first solved with different regularization parameters, following which the solution with appropriate regression error and cardinality will be selected [16]. The major advantage of LASSO method is its computational efficiency (a convex optimization) even for a very large signal reconstruction problem.

3. Measured Signals and Signal Analysis

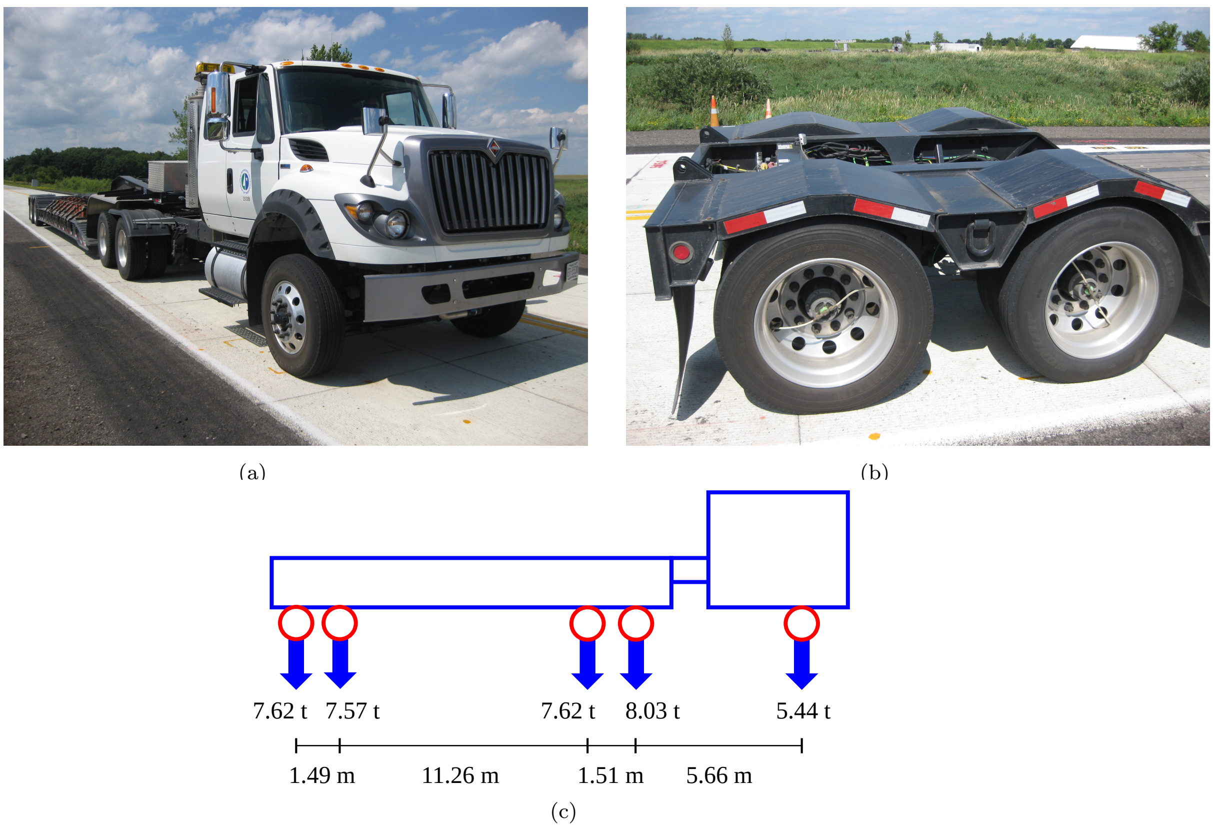

Figure 2: MnROAD Truck and its axle layout details. (a) MnROAD Truck; (b) tandem; (c) layout of axle loads and axle distances.

To investigate the effectiveness of the CS methods in traffic data analysis for vehicle axle detection, data collected at varied sampling frequencies is needed. In this paper, the actual data to be analyzed were measured from the strain gauge and fiber-Bragg-grating (FBG) sensors pre-installed in the concrete panel at the Minnesota Cold Weather Road Research Facility (MnROAD) from Minnesota Department of Transportation (MnDOT). As shown in Fig. 1(a), the MnROAD Facility has two separte roadways: (1) a two-lane low-volume loop with a 80,000 lb semi-truck (i.e., the MnROAD Truck) load; (2) a road section of the interstate I-94 containing two westbound lanes loaded with live traffic vehicles. Fig. 1(b) displays a road section of the Cell 40. Cell 40 is comprised of concrete pavements which have a panel dimension of 6 ft $\times$ 6 ft $\times$ 3 in. The concrete pavement is embedded with GFRP-packaged FBG sensors, strain gauges, etc. for pavement health condition and performance monitoring as well as traffic analysis. Figs. 2 (a) and (b) demonstrate the MnROAD Truck for axle detection tests and the rear tandem, respectively. Fig. 2 (c) shows the detailed information of axle loads. More details can be found in [5, 6, 18, 19].

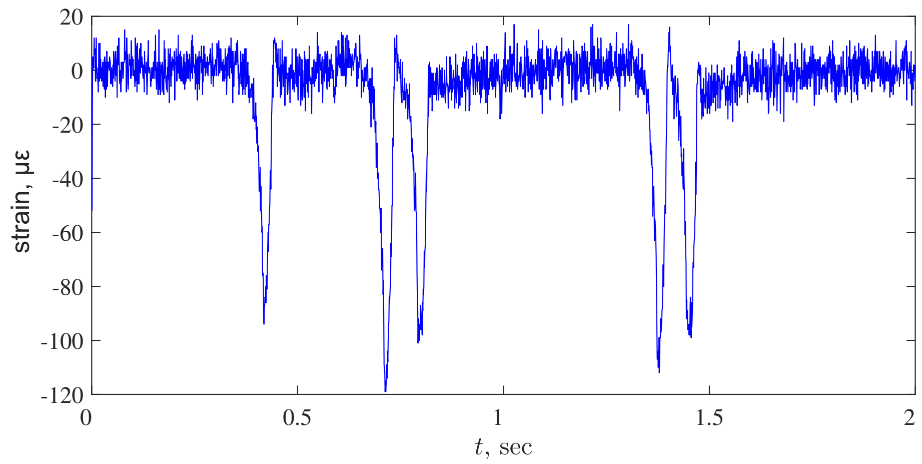

Figure 3: An example strain signal. The sampling rate is $f_s = 1200$ Hz; the vehicle speed is $v = 39$ mph.

With a sufficient sampling frequency, a measurement device can capture the strain pulse for each axle as the truck travels across the pavement panels installed with sensors. Zhang et al. [5] concluded from related signal analysis that the signal's fundamental bandwidth required for accurate measurements increases with the vehicle's traveling speed. Fig. 3 shows the signal measured using the in-pavement strain gauge. The corresponding vehicle speed is 39 mph, and the sampling frequency is 1200 Hz. With a sampling frequency as high as 1200 Hz, the measured signal in Fig. 3 shows clearly the crossing of each truck axle with a an apparent pulse.

Unlike from signal measurement for the strain gauge, the data collection device for the FBG sensor (i.e., NI PXIe-4844 Optical Sensor Interrogator) had a sampling frequency as low as 10 Hz. This low sampling frequency of the installed FBG sensors limits their application in high-speed traffic data collection. However, it provides an opportunity to examine the data in hand for more information than it supplies directly. Figs. 4 (a) to (f) show plots of the measured signals from the FBG sensor with a sampling frequency of 10 Hz for the

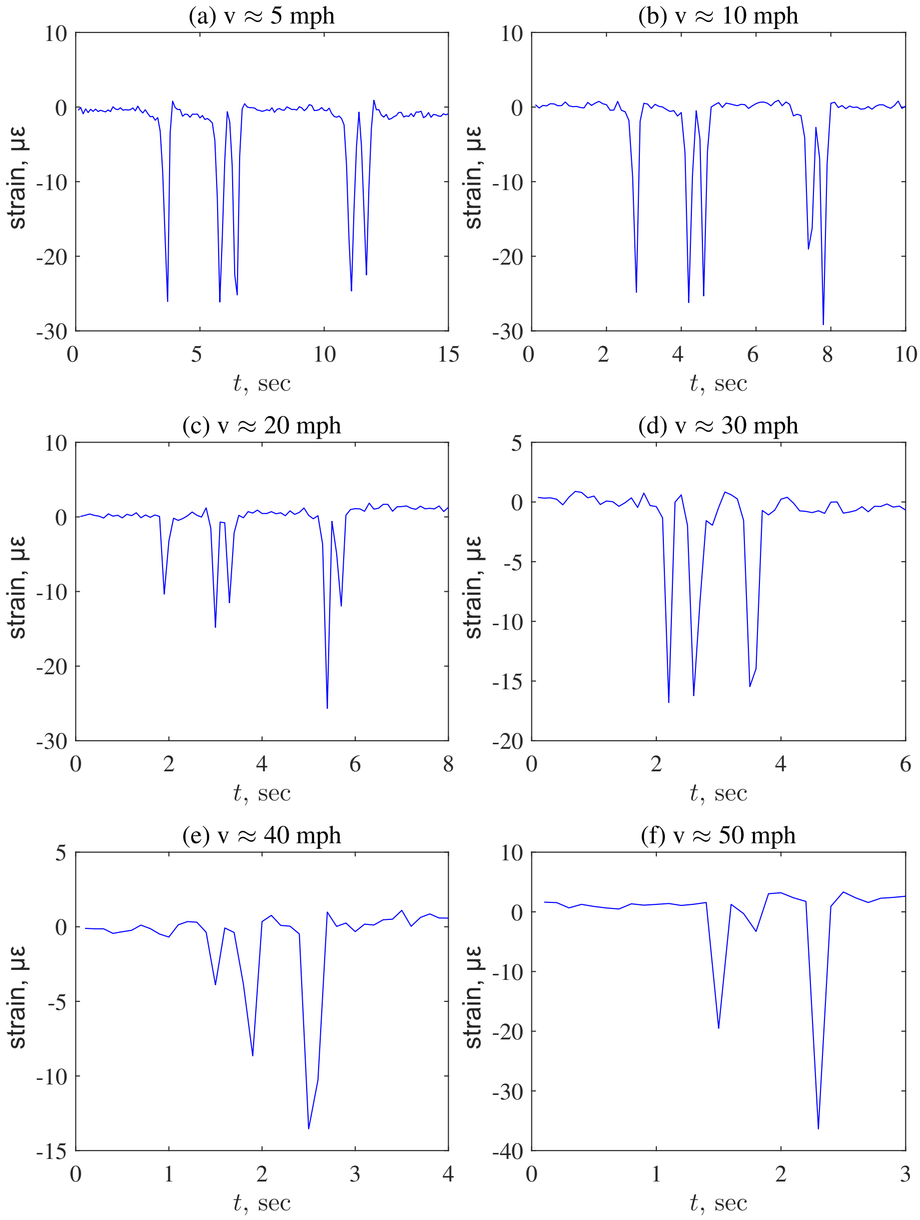

Figure 4: Collected signals from the FBG sensor. The sampling frequency is $f_s = 10$ Hz.

traversals with vehicle speed varying from 5 mph to 50 mph. The speed was controlled by a truck driver and thus was approximate. The strains measured by the FBG sensor have lower magnitudes than that from the strain gauge mainly because of their differences in the installation locations and positions within the pavement panel. Unrepeatable driving routes also contributed to the variance in measurement. Furthermore, under-sampling caused signal attenuation [5]. Additionally, the hardware associated with the FBG sensor provided a higher SNR in signal collection and transmission than the strain gauge.

Fig. 4 (a) shows the signal pulses produced when the truck travels at a low speed of

Table 1: Measured pulse widths through peak-finding

vehicle speed v , mph	sampling frequency f, Hz	pulse 1 , m	pulse 2 , m	pulse 3 , m	pulse 4 , m	pulse 5 , m
5	10	0.47	0.54	0.52	0.62	0.49
10	10	0.61	0.66	0.55	0.87	0.62
20	10	1.22	1.05	0.97	1.04	1.13
30	10	1.47	2.25	2.76	-	-
40	10	1.86	2.62	3.38	-	-
50	10	2.34	2.50	2.35	-	-
39	1200*	0.42	0.46	0.43	0.50	0.48

* strain gauge

$v \approx 5$ mph across the instrumented pavement. The sampling frequency of 10 Hz is close to the frequency of 13 Hz recommended in [5] for a traversal of 5 mph. As the speed increases, the signal power shifts further into the high-frequency band. However, a low sampling frequency excludes the high-frequency components that are necessary for producing sharper signal transitions. Consequently, under-sampling the signal causes signal distortion by widened and merging pulses [5]. The gradual variation of signal widths in Figs. 4 (b) to (f) emphasizes this phenomenon. All five pulses remain identifiable when $v \approx 10$ mph and $v \approx 20$ mph. However, distortion begins to merge the pulses for the tandem axles. Further increases in speed result in severe distortion such that the pulses for tandems axles merge into one pulse, from which it is rather difficult to identify the passage of two axles.

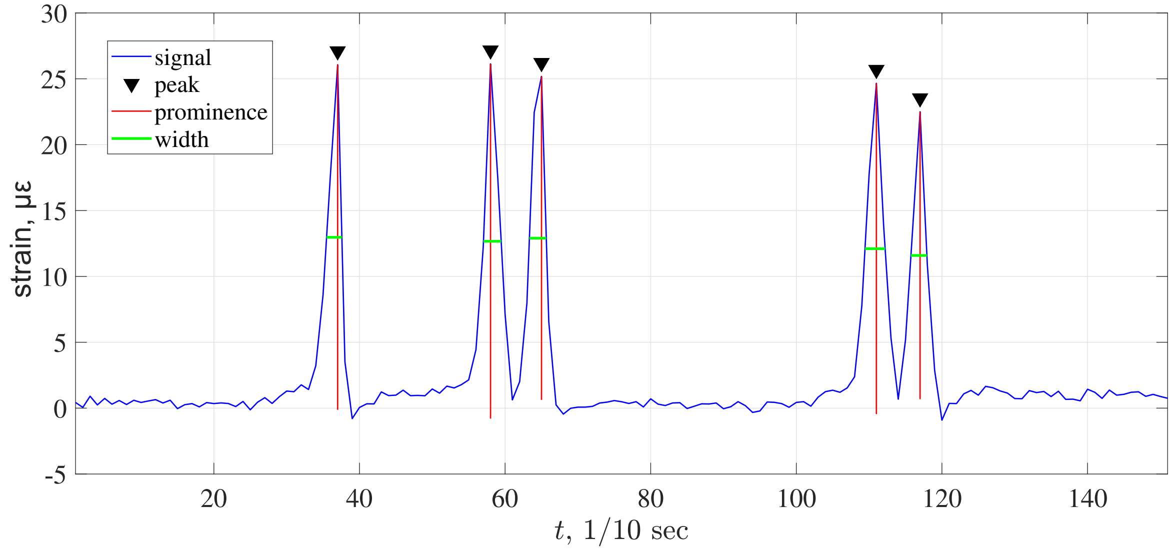

Figure 5: Example of peak-finding using the "*findpeaks*" function in MATLAB. The signal is the strain from the FBG sensor with $v \approx 5$ mph. The signal width is measured at half prominence.

Zhang et al. [5] quantified signal distortion from under-sampling by the pulse width at its half prominence. The embedded function "*findpeaks*" in MATLAB locates the local maxima and graphically illustrates their prominence and width. Fig. 5 shows the results of peak-finding using the strain signal in Fig. 4 (a). The sign of the signal is inverted for the convenience of applying the "*findpeaks*" function in MATLAB. Table 1 compares the measured pulse widths. The last row lists the pulse widths of the strain gauge signal as a reference due to its sufficiency in sampling frequency. Compared with the strain gauge signal, the pulse widths of the FBG signal at $v \approx 5$ mph is slightly higher because of the lower sampling frequency. The pulses are widened gradually, though not proportionally, with the increase of speed. At $v \approx 30$ mph, as the tandem pulses merge, the width of pulse 2 is larger than the sum of the widths of pulses 2 and 3 for $v \approx 20$ mph. The phenomenon repeats with pulse 3, which has a width exceeding that of pulses 4 and 5 summed for $v \approx 20$ mph. The pulse widths for $v \approx 40$ mph increase further compared with that for $v \approx 30$ mph. When the speed increases further to 50 mph, the pulse widths vary inconsistently, most probably due to severe signal distortion and attenuation. For relative comparison, Table 2 lists the ratios of pulse widths to that for $v \approx 5$ mph.

Table 2: Ratios of pulse widths taking the case with $v \approx 5$ mph as reference

vehicle speed v , mph	sampling frequency f, Hz	pulse 1	pulse 2	pulse 3	pulse 4	pulse 5
5	10	1	1	1	1	1
10	10	1.3	1.2	1.1	1.4	1.3
20	10	2.6	1.9	1.9	1.7	2.3
30	10	3.1	4.1	5.3	-	-
40	10	4.0	4.8	6.5	-	-
50	10	5.0	4.6	4.5	-	-

4. Signal Recovery for Axle Detection: the Problem Formulation and Trial Analysis

Section 3 clearly shows that insufficient sampling frequency will lead to the loss of detection in vehicle axle at high driving speeds. To recover the signal components important for vehicle axle detection from the imprecisely measured signals, this section formulates the CS method of signal recovery and tests its effectiveness using a sufficiently sampled signal. Section 4.1 formulates the sensing matrix, Φ, for recovering the signal pulses referring to the results of the signal analysis in Section 3. Section 4.2 tests the performance of signal recovery of the CS method with the strain gauge signal measured at $f_s = 1200$ Hz.

4.1. Sensing Matrix Formulation

In this study, for signal recovery, the sensing matrix is formulated in the same way as in the authors' previous study [9]. The sensing matrix simulates the decimation operation of a low-pass anti-aliasing filter in a practical measuring device, as shown in Fig. 6. As a result, the sensing matrix Φ in CS should incorporate the lowpass filtering ($\widetilde{H}$) and digitizing (D), so that $\Phi = \widetilde{H} \times D$, in which

$$\widetilde{H} = \begin{bmatrix} h_{\mathrm{d}}[0] & 0 & 0 & \dots & 0 & 0 & 0 & 0 \\ h_{\mathrm{d}}[1] & h_{\mathrm{d}}[0] & 0 & \dots & 0 & 0 & 0 & 0 \\ \dots & \dots & \dots & \dots & \dots & \dots & \dots & \dots \\ h_{\mathrm{d}}[N_2-1] & h_{\mathrm{d}}[N_2-2] & \dots & h_{\mathrm{d}}[0] & 0 & \dots & 0 & 0 \\ 0 & h_{\mathrm{d}}[N_2-1] & h_{\mathrm{d}}[N_2-2] & \dots & h_{\mathrm{d}}[0] & 0 & \dots & 0 \\ \dots & \dots & \dots & \dots & \dots & \dots & \dots & \dots \\ 0 & 0 & \dots & \dots & \dots & 0 & h_{\mathrm{d}}[N_2-1] & h_{\mathrm{d}}[N_2-2] \\ 0 & 0 & \dots & \dots & \dots & \dots & 0 & h_{\mathrm{d}}[N_2-1] \end{bmatrix}_{(N_1+N_2-1)\times N_1} \tag{1}$$

$$D = \begin{bmatrix} 1 & 0 & 0 & 0 & 0 & \dots & 0 & 0 \\ 0 & 0 & 0 & 1 & 0 & \dots & 0 & 0 \\ \dots & \dots & \dots & \dots & \dots & \dots & \dots & \dots \\ 0 & 0 & 0 & 0 & 0 & \dots & 0 & 1 \end{bmatrix}_{(N_1/3)\times(N_1+N_2-1)} \tag{2}$$

$\hat{h}_{\mathrm{d}}[n]$ is the impulse response of the low pass filter, and N_1 and N_2 denote the length of $x[n]$ and $h_{\mathrm{d}}[n]$, respectively. More details about the formulation of the sensing matrix can be found in [9].

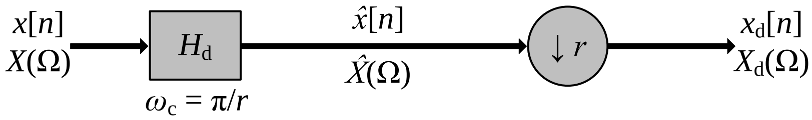

Figure 6: Block representation of decimation (Reproduced from [20]). $x[n]$ is the original signal, $X(\Omega)$ represents the counterpart of $x[n]$ in the frequency domain, H_{d} represents the low-pass filter, ω_c is the cutoff frequency, r is the decimation factor, $\hat{x}[n]$ denotes the filtered signal with $\hat{X}(\Omega)$ being its counterpart in the frequency domain, $x_{\mathrm{d}}[n]$ and $X_{\mathrm{d}}(\Omega)$ denote the decimator outputs.

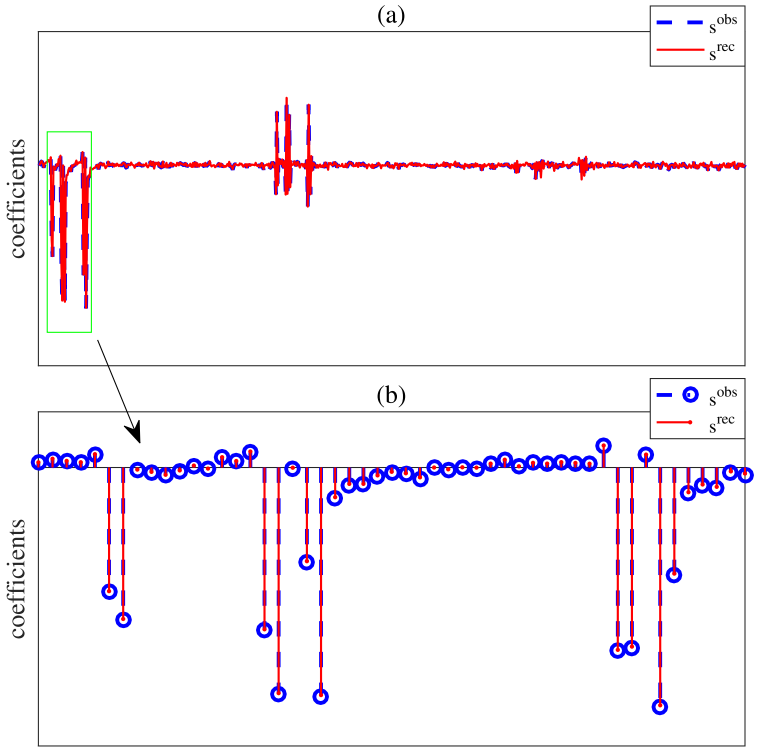

Figure 7: Coefficients of wavelet decomposed strain gauge signal in Fig. 9 (a) using the wavelet basis 'db4' and the recovered coefficients using the LASSO method from the decimated signal in Fig. 9 (b).

175 *4.2. Trial Analysis with the Strain Gauge Signal*

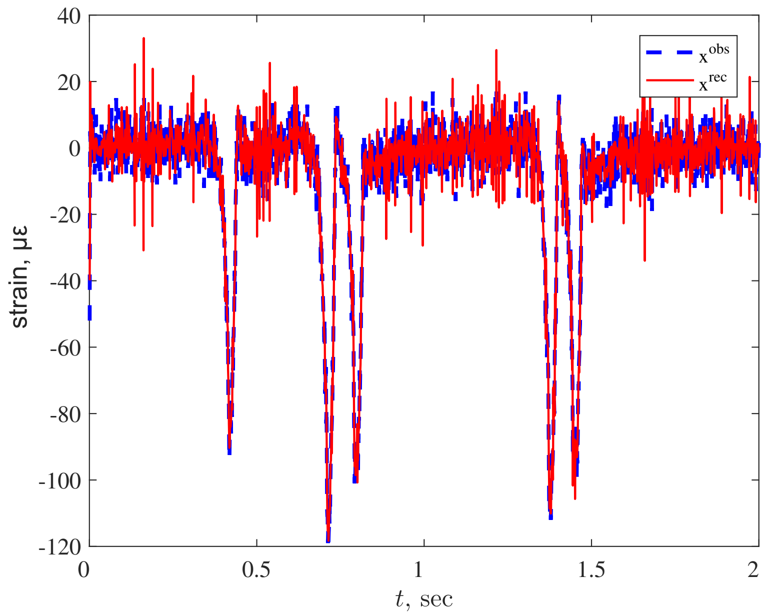

Figure 8: Comparison of the recovered strain signal x^{rec} with the measured signal x^{obs}.

This section analyzes the strain signal measured with sufficient sampling frequencies to evaluate the potential of CS for signal recovery from under-sampling measurement. Here, "sufficient" sampling signifies that the measured signal has significant pulses for direct axle detection through peak-finding. The trial analysis uses the strain data that are measured from strain gauge at a sampling rate of $f_s = 1200$ Hz with vehicle traveling at $v = 39$ mph (Fig. 3). Without loss of generality, the decimation factor is set to $r = 2$ and the LASSO method is used for signal recovery.

Figs. 9 (a) and (b) compare the measured signal from strain gauge and the results of decimation. The lowpass filter in decimation reduces the noise level and thus improves the SNR. As the strain signal is not sparse itself, this study expands the measured signal using the wavelet transform to represent it by a sparse vector of coefficients. Test analysis shows that the wavelet basis 'db4' from the Daubechies wavelet family yields a sparse representation of the measured signal when it is decomposed to the 5^{th} level. The LASSO algorithm of CS takes the decimated signal, the sensing matrix Φ, and the expansion matrix Ψ as inputs and sets the sparse coefficients s as the target of signal recovery.

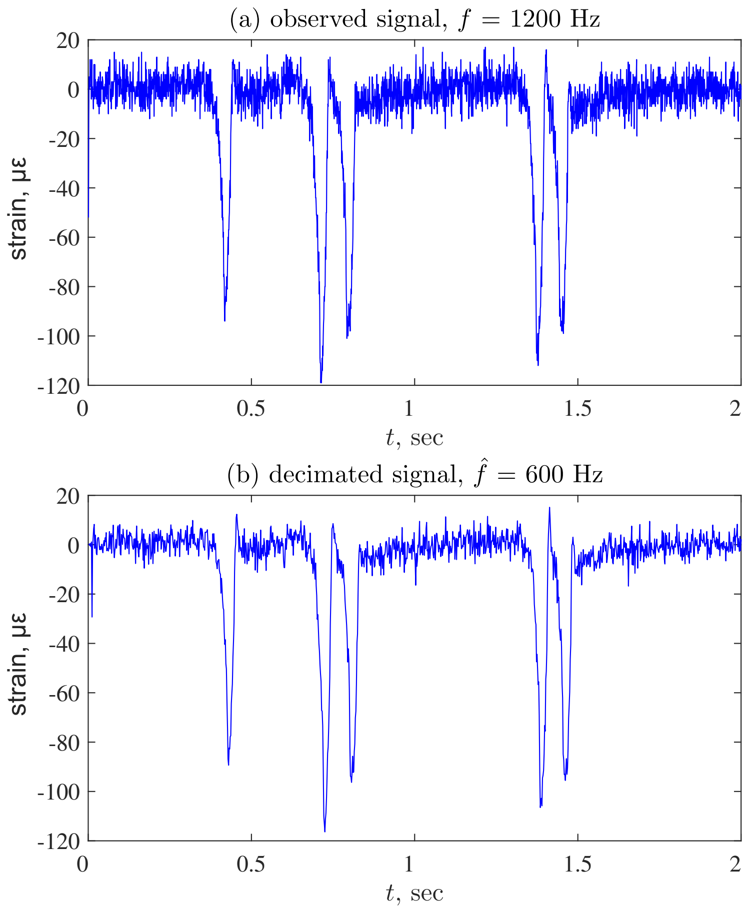

Figure 9: Strain signal at $f_s = 1200$ Hz and its decimation with $r = 2$.

Figs. 7 (a) and (b) compare the coefficients of the measured signal made sparse using the 'db4' wavelets, s^{obs}, and the coefficients recovered using the LASSO method, s^{rec}. The comparison shows high quality of recovery with little deviation of s^{rec} from s^{obs}. Fig. 8 compares the measured strain signal, x^{obs}, and the recovered signal, x^{rec}, from the decimated signal with $x^{\mathrm{rec}} = \Psi s^{\mathrm{rec}}$, which also shows high consistency. The encouraging outcomes of signal recovery shown in Figs 7 and 8 evidences the potential for recovering a signal from its under-sampling measurement using the CS based method. The rest of this paper will examine the quality of signal recovery from measured signals with insufficient sampling frequency.

Table 3: Recognized axle distances through peak-finding (CoSaMP)

vehicle speed v , mph	sampling frequency f or $\hat{f}$, Hz	axle distance 1 AD_1, sample	axle distance 2 AD_2, sample	axle distance 3 AD_3, sample	axle distance 4 AD_4, sample
5	10	21	7	46	6
10	10	14	4	28	4
20	10	11	3	21	3
30	10	4	9	-	-
40	10	4	6	-	-
50	10	3	5	-	-
30	20*	8	2	16	2
40	30*	10	3	18	3
50	20*	16	19	2	-
39	1200**	353	96	703	93

* pseudo sampling frequency; ** strain gauge

5. Signal Recovery for Axle Detection: CS from Under-Sampled Signals

This section shows the outcome of signal recovery using the two CS methods and evaluates their effectiveness in axle detection. Sections 5.1 and 5.2 show the outcome of signal recovery using under-sampled data for vehicle axle detection using the CoSaMP and LASSO methods, respectively. This paper obviates elaborating these two methods due to the limited length. The authors refer to [15] for details on the development of CoSaMP, and to [16] for details on the LASSO method.

5.1. Signal Recovery using the CoSaMP method

In this section, the results of signal recovery with under-sampled signals from FBG sensor using the CoSaMP method of CS are presented. The investigated vehicle speeds are $v \approx 30$ mph, $v \approx 40$ mph, and $v \approx 50$ mph . To determine the best configuration for CS using the CoSaMP method, the influence of two parameters is investigated: (1) the ratio of decimation r that determines the pseudo-sampling-frequency $\hat{f}_{\mathrm{s}}$ of the recovered signal and the sensing matrix Φ; and (2) the target sparsity κ_{t} that specifies the number of non-zero data in the recovered signal. The criteria include the normalized error in signal recovery, R_{norm}, and

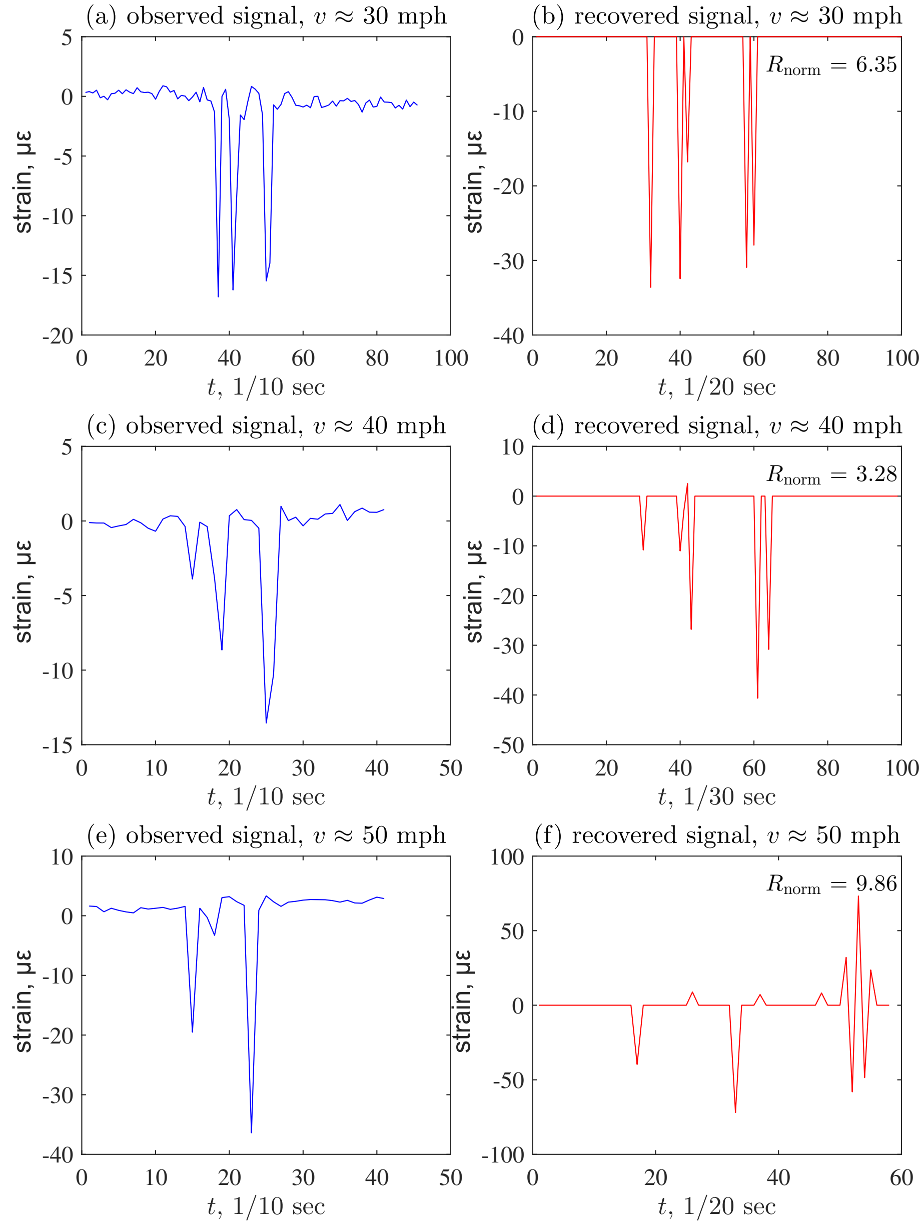

Figure 10: Recovered signals using the CoSaMP algorithm with observed signals collected at different vehicle traveling speeds. For case $v \approx 30$ mph: $r_{\text{us}} = 2$ and $\kappa_{\text{t}} = 5$; for case $v \approx 40$ mph: $r = 3$ and $\kappa_{\text{t}} = 7$; for case $v \approx 50$ mph: $r = 2$ and $\kappa_{\text{t}} = 10$.

the sparsity of recovered signal. It should be noted that in this section and in Section 5.2, wavelet expansion is unnecessary because the target of signal recovery x is already sparse. Subsequently, the analysis ignores the matrix Ψ.

Intensive parametric analysis reveals the optimum settings of the CoSaMP method, when it reaches the balance between the reovery error and signal sparsity. That is $r = 3$ and $\kappa_{\text{t}} = 5$ for $v \approx 30$ mph, $r = 3$ and $\kappa_{\text{t}} = 7$ for $v \approx 40$ mph, and $r = 2$ and $\kappa_{\text{t}} = 10$ for $v \approx 50$ mph.

Table 4: Ratios of axle distance taking AD1 as reference (CoSaMP)

vehicle speed v , mph	sampling frequency f or $\hat{f}$, Hz	axle distance 1 AD_1	axle distance 2 AD_2	axle distance 3 AD_3	axle distance 4 AD_4
5	10	1	0.3	2.2	0.3
10	10	1	0.3	2.0	0.3
20	10	1	0.3	1.9	0.3
30	10	1	2.3	-	-
40	10	1	1.5	-	-
50	10	1	1.7	-	-
30	20*	1	0.3	2.0	0.3
40	30*	1	0.3	1.8	0.3
50	20*	1	1.2	0.1	-
39	1200**	1	0.3	2.0	0.3
-	***	1	0.3	2.0	0.3

* pseudo sampling frequency; ** strain gauge; *** direct measurement from Fig. 2 (c).

Fig. 10 shows the results of signal recovery for the three speed cases. It can be seen that CS recovers all the five pulses for the case with $v \approx 30$ mph and $v \approx 40$ mph. However, it fails to recognize the adjacent pulses for the first tandem for the case with $v \approx 50$ mph, most probably due to the excessive severity of signal distortion caused by insufficient sampling frequency. Previous study [5] by authors of the present paper recommends a sampling frequency of 128 Hz for $v = 50$ mph according to the Nyquist sampling theorem, which is much higher than that available (i.e., 10 Hz) in measuring the FBG signal. Figs. 11 (a) to (c) compare the measured signals b^{obs} with that recovered by CS, b^{rec}. The two curves matches well in all three plots. Fig. 11 (c) shows that although the CS is accurate in the sense that the recovered signal is a solution of the problem $Ax = b$, it does not yield the identical x to the target source signal with recognizable pulses for all vehicle axles.

To evaluate the accuracy of signal recovery for axle detection, Tables 3 and 4 compare the axle distances, i.e., the distances between pulses, and their ratios of the recovered signal by CS with that identified from the measured signals. As introduced in Section 3, the peak-finding technique provides the axle distances. Table 4 shows that for the cases with $v \approx 30$ mph and $v \approx 40$ mph, the recovered signals represent axle distances with very close ratios to that from the FBG signals with $v \approx 5$ mph, $v \approx 10$ mph, and $v \approx 20$ mph, the strain gauge signal, and direct measurement in Fig. 2 (c). This consistency of axle distance ratios verifies the effectiveness of recovering signal with the CoSaMP method for the purpose of axle detection, excluding the possibility of recovering random pulses from the measured signal.

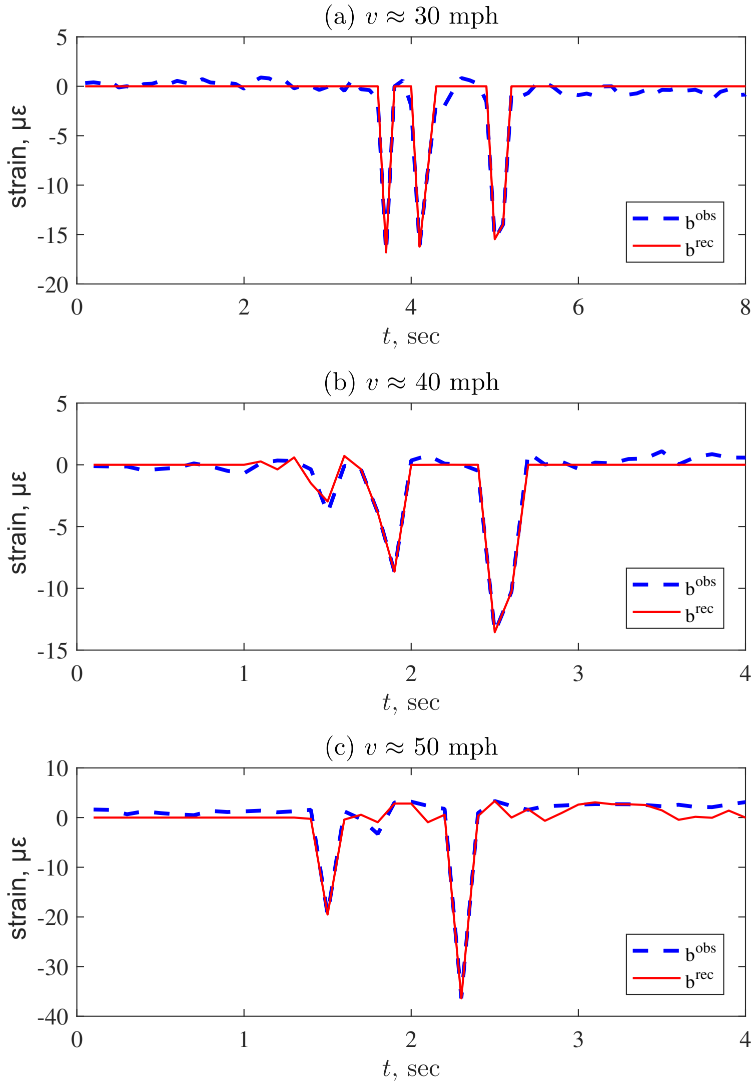

Figure 11: Comparison of observed signal b^{obs} with its reconstruction b^{rec} from $b^{\text{rec}} = \Phi x^{\text{rec}}$. Φ is the sensing matrix; x^{rec} is the recovered signal using the CoSaMP algorithm from Φ and b^{obs}.

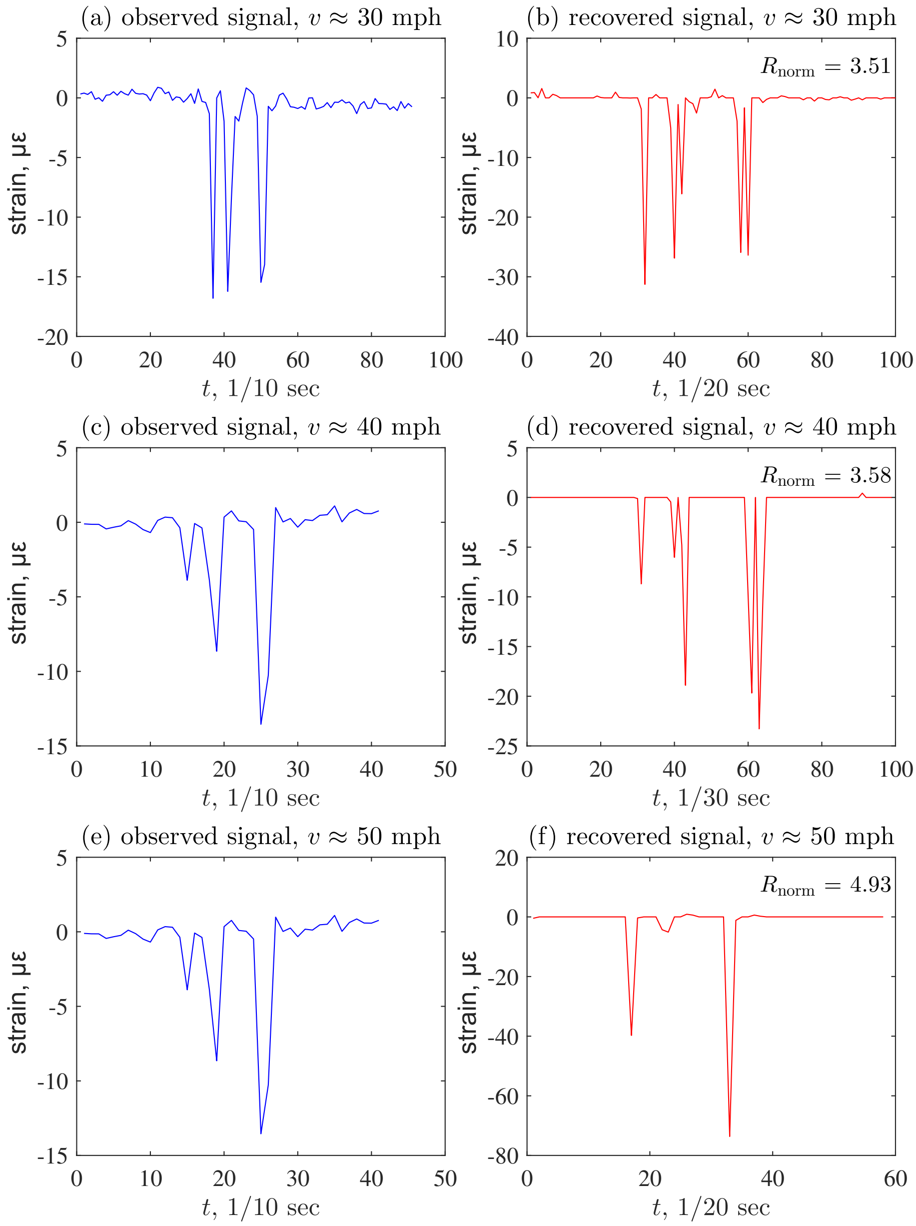

Figure 12: Recovered signal using the LASSO algorithm with observed signal collected at different vehicle traveling speeds. For case $v \approx 30$ mph: $r_{\text{us}} = 2$; for case $v \approx 40$ mph: $r_{\text{us}} = 3$; for case $v \approx 50$ mph: $r_{\text{us}} = 2$.

5.2. Signal Recovery using the LASSO method

This section show the outcome of recovering signal for axle detection using the LASSO method. The same setting of decimation factor when formulating the sensing matrix as optimized in Section 5.1 is used in this section. The LASSO method does not necessarily require passing a target sparsity (i.e., κ_t as in the CoSaMP method). Instead, it gives the results of signal recovery for a series of sparsity and the corresponding residuals. Referring to [21], this study selects the CS results at the diminishing point of the residual curve that has a relative low sparsity; in other words, the determination of the CS-recovered signal in LASSO is the result of balancing the error (R_{norm}) and sparsity.

Table 5: Recognized axle distances through peak-finding (LASSO)

vehicle speed v , mph	sampling frequency f or $\hat{f}$, Hz	axle distance 1 AD_1, sample	axle distance 2 AD_2, sample	axle distance 3 AD_3, sample	axle distance 4 AD_4, sample
5	10	21	7	46	6
10	10	14	4	28	4
20	10	11	3	21	3
30	10	4	9	-	-
40	10	4	6	-	-
50	10	3	5	-	-
30	20*	8	2	16	2
40	30*	9	3	18	2
50	20*	6	10	-	-
39	1200**	353	96	703	93

* pseudo sampling frequency; ** strain gauge

Figs. 12 shows the results of CS using the LASSO method for FBG signals at $v \approx 30$ mph, $v \approx 40$ mph, and $v \approx 50$ mph. Similar to the results of the CoSaMP method, the LASSO method for signals at $v \approx 30$ mph and $v \approx 40$ mph yields signals with apparent pulses corresponding to the passage of all truck axles, but it fails to recover an efficient signal for axle detection from the signal at $v \approx 50$ mph. The normalized residuals are at the same level with that of the CoSaMP method. As expected, the recovered signal shows high consistency with the measured signal as shown in Fig. 13. Tables. 5 and 6 compare the axle distances and their ratios identified from the signal pulses. Similar to the CoSaMP method, the LASSO method generates signals with axle distance ratios close to the references for the cases with $v \approx 30$ mph and $v \approx 40$ mph. In summary, the LASSO method produces encouraging results of signal recovery for axle detection, as did the CoSaMP method.

6. Conclusions

Since insufficient sampling could distort and attenuate the signal pulses and thus reduce the accuracy of axle detection, this study investigates the compressed sensing (CS) methods, specifically, CoSaMP and LASSO methods, to recover the important signal pulses for vehicle axle detection from under-sampling measurements. The case study used strain signals collected from inside-pavement installed sensors. CS requires formulating sensing matrix and expansion matrix for sparse representation. This study uses decimation to model the effects of signal under-sampling, which results from low-pass filtering and digitizing, to derive the sensing matrix for signal recovery. For signals measured with a sufficient sampling frequency, a wavelet basis is effective in expanding the signal into sparse representation, which then forms the expansion matrix in CS. Trial analysis using the sufficiently measured signal from the strain gauge shows the potential for using CS methods to recover the essential signal pulses essential for vehicle axle detection and hence lays the foundation for signal recovery from the under-sampled signals. From the case study, it can be seen that the two CS methods, CoSaMP and LASSO, can recover signals from under-sampling measurements as long as the vehicle speed corresponding to the measured signal is not excessively higher than the measuring scope of the sampling equipment according to the Nyquist theorem.

Table 6: Ratios of axle distance taking AD1 as reference (LASSO)

vehicle speed v , mph	sampling frequency f or $\hat{f}$, Hz	axle distance 1 AD_1	axle distance 2 AD_2	axle distance 3 AD_3	axle distance 4 AD_4
5	10	1	0.3	2.2	0.3
10	10	1	0.3	2.0	0.3
20	10	1	0.3	1.9	0.3
30	10	1	2.3	-	-
40	10	1	1.5	-	-
50	10	1	1.7	-	-
30	20*	1	0.3	2.0	0.3
40	30*	1	0.3	2.0	0.2
50	20*	1	1.7	-	-
39	1200**	1	0.3	2.0	0.3
-	***	1	0.3	2.0	0.3

* pseudo sampling frequency; ** strain gauge; *** direct measurement from Fig. 2 (c).

The results of this paper have the potential to reduce the cost in traffic data analysis and make full use of available measurement equipment especially in case of emergency. This analysis was limited to strain data collected from in-pavement sensors. However, practitioners can extend this concept to other measurements for traffic data collection.

Acknowledgments

The authors acknowledge the technical assistance from Robert Strommen, etc. at MnROAD facility, MnDOT, MN, during the field tests.

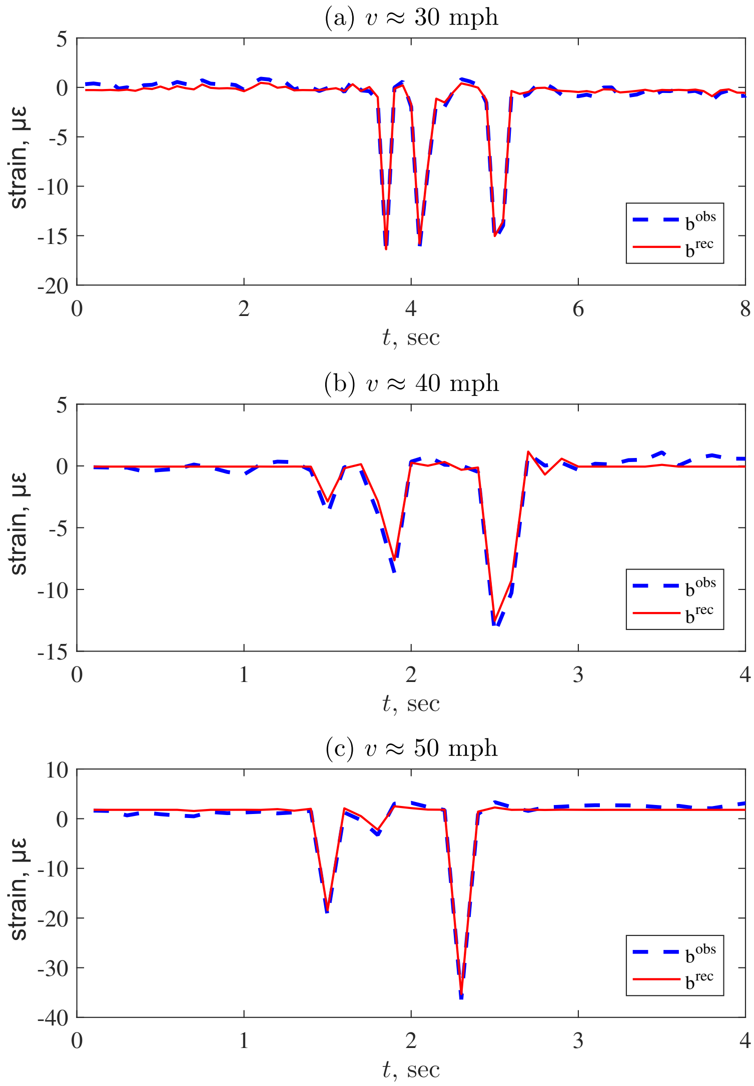

Figure 13: Comparison of observed signal b^{obs} with its reconstruction b^{rec} from $b^{\text{rec}} = \Phi x^{\text{rec}}$. Φ is the sensing matrix; x^{rec} is the recovered signal using the LASSO algorithm from Φ and b^{obs}.

References

[1] W. Zhang, Q. Wang, C. Suo, A novel vehicle classification using embedded strain gauge sensors, Sensors 8 (11) (2008) 6952–6971.

[2] W. Xue, D. Wang, L. Wang, Monitoring the speed, configurations, and weight of vehicles using an in-situ wireless sensing network, IEEE Transactions on Intelligent Transportation Systems 16 (4) (2015) 1667–1675.

[3] M. Al-Tarawneh, Y. Huang, P. Lu, D. Tolliver, Vehicle classification system using in-pavement fiber bragg grating sensors, IEEE Sensors Journal 18 (7) (2018) 2807–2815.

[4] Y. Huang, et al., In-pavement fiber bragg grating sensors for high-speed weigh-in-motion measurements, in: Sensors and Smart Structures Technologies for Civil, Mechanical, and Aerospace Systems 2017, Vol. 10168, International Society for Optics and Photonics, 2017, p. 101681Y.

[5] Z. Zhang, Y. Huang, R. Bridgelall, L. Palek, R. Strommen, Sampling optimization for high-speed weigh-

in-motion measurements using in-pavement strain-based sensors, Measurement Science and Technology 26 (6) (2015) 065003.
[6] Z. Zhang, Y. Huang, R. Bridgelall, P. Lu, et al., Optimal system design for weigh-in-motion measurements using in-pavement strain sensors, IEEE Sensors Journal 17 (23) (2017) 7677–7684.
[7] D. L. Donoho, Compressed sensing, IEEE Transactions on information theory 52 (4) (2006) 1289–1306.
[8] E. J. Candès, J. Romberg, T. Tao, Robust uncertainty principles: Exact signal reconstruction from highly incomplete frequency information, IEEE Transactions on information theory 52 (2) (2006) 489–509.
[9] Z. Zhang, C. Sun, Y. Huang, Sparse signal recovery for WIM measurements from undersampled data through compressed sensing, Measurement 151 (2020) 107181.
[10] H. Sousa, Y. Wang, Sparse representation approach to data compression for strain-based traffic load monitoring: A comparative study, Measurement 122 (2018) 630–637.
[11] E. J. Candes, J. K. Romberg, Signal recovery from random projections, in: Computational Imaging III, Vol. 5674, International Society for Optics and Photonics, 2005, pp. 76–87.
[12] E. J. Candes, J. K. Romberg, T. Tao, Stable signal recovery from incomplete and inaccurate measurements, Communications on Pure and Applied Mathematics: A Journal Issued by the Courant Institute of Mathematical Sciences 59 (8) (2006) 1207–1223.
[13] L. Zhu, J. H. McClellan, Compressive sensing based intercell interference channel estimation for heterogeneous network, in: Signal Processing Advances in Wireless Communications (SPAWC), 2014 IEEE 15th International Workshop on, IEEE, 2014, pp. 429–433.
[14] K. J.-L. Pan, L. Zhu, T. Haque, J. H. McClellan, An enhanced compressed sensing-based interference-resistant receiver for lte systems, in: Vehicular Technology Conference (VTC Spring), 2015 IEEE 81st, IEEE, 2015, pp. 1–5.
[15] D. Needell, J. A. Tropp, Cosamp: Iterative signal recovery from incomplete and inaccurate samples, Applied and computational harmonic analysis 26 (3) (2009) 301–321.
[16] N. Boyko, G. Karamemis, V. Kuzmenko, S. Uryasev, Sparse signal reconstruction: Lasso and cardinality approaches, in: Dynamics of Information Systems, Springer, 2014, pp. 77–90.
[17] A. C. Gilbert, M. J. Strauss, J. A. Tropp, R. Vershynin, One sketch for all: fast algorithms for compressed sensing, in: Proceedings of the thirty-ninth annual ACM symposium on Theory of computing, ACM, 2007, pp. 237–246.
[18] Z. Zhang, F. Deng, Y. Huang, R. Bridgelall, Road roughness evaluation using in-pavement strain sensors, Smart Materials and Structures 24 (11) (2015) 115029.
[19] Z. Zhang, Y. Huang, L. Palek, R. Strommen, Glass fiber–reinforced polymer–packaged fiber bragg grating sensors for ultra-thin unbonded concrete overlay monitoring, Structural Health Monitoring 14 (1) (2015) 110–123.
[20] B. P. Lathi, R. A. Green, Essentials of digital signal processing, Cambridge University Press, 2014.
[21] R. Hou, Y. Xia, X. Zhou, Structural damage detection based on l1 regularization using natural frequencies and mode shapes, Structural Control and Health Monitoring 25 (3) (2018) e2107.